Memoirs of the Scientific Sections of the Romanian Academy
Tome XXXVI, 2013

CHEMISTRY

POLY(AMIDEHYDROXYURETHANE) TEMPLATE MAGNETITE NPS ELECTROSYNTHESIS. II. CORE AND SHELL CHARACTERIZATION

LAURA URSU

Advanced Research Center for Bionanoconjugates and Biopolymers,
"Petru Poni" Institute of Macromolecular Chemistry
E-mail: ursu.laura@icmpp.ro

Core and layer polymer characterization of magnetite nanoparticles (NPs) surface-functionalized with poly(amidehydroxyurethane) (PAmHU), obtained by a new electrochemical synthesis route is presented. The core magnetic properties were investigated by Vibrating Sample Magnetometer (VSM), showing that the obtained NPs have superparamagnetic to ferromagnetic behaviour (very low coercivity and remanence). The magnetite–PAmHU NPs morphology and size were studied by Atomic Force Microscopy (AFM) and Dynamic Light Scattering (DLS); both methods showed the existence of PAmHU out-flaked layer on NPs. Structural analysis by Infrared spectroscopy (FTIR) and Thermogravimetry (TG) confirm the out-flaking of magnetic NPs with PAmHU.

Key words: magnetite–PAmHU capped NPs, core and shell characterization.

1. INTRODUCTION

Functional nanostructures consisting of magnetic crystallites encapsulated in polymer matrices possess features and capabilities with a great potential for applications in electromagnetic interference shielding, magneto-optical storage and flexible electronics [7], biomedical sensing [1], drug delivery carrier [4], biological separation [19], *in vivo* magnetic resonance imaging [18], hyperthermia [8], etc.

The ideal NPs for biomedical applications should have diameters of about 5–400 nm, dimensions comparable with size of biologically important entities, together with a good biocompatibility [3]. Biocompatibility requires the use of nanoparticles coated or dispersed/embedded in a polymer with good solubility and tolerance in aqueous biological fluids and/or at interface with cells or tissues. Both natural and synthetic polymers have been used to produce thus functionalized magnetic NPs [10]. Usually, the magnetic-polymer coated, out-flanked or shielded NPs are obtained in two steps. The first step consists in the synthesis process of NPs in which the particles size, the crystals symmetry, etc. are controlled [11], after which, in the second step the NPs are capped with polymer. A good efficiency is obtained during the one step synthesis of functionalized NPs–polymer conjugates

but, generally, this type of synthesis leads to a decrease in the amount of nanoparticle material per unit volume, an increase in the particles size and also an increase in the polydispersity of the NPs.

We developed a new synthesis route by combining the tunability of PAmHU water–soluble polymer, used as restricted reaction room support (host), with the electrochemical reduction of Fe metal ions in a galvanostatic process; the proton source is the hydrogen released from cathode electrolysis process [14]. This route has major advantages due to the fact that the control of the particles size can be done by the current of the galvanostatic process, the polymer composition, pH and temperature.

The chemical identification by Electron Spectroscopy for Chemical Analysis (ESCA), Electron Paramagnetic Resonance measurements (EPR) and X-ray diffraction (XRD) revealed that the NPs form a PAmHU–clustering system with an inner-core consisting of magnetite crystallite unit entities [14]. Dimensional analysis by Scherrer method showed that the crystallites have irregular shapes of tens of nanometres.

The objectives of this study are the characterization of magnetite inner core and PAmHU out-layer of NPs cluster systems by complementary methods in order to consider them suitable for applications.

2. EXPERIMENTAL

Materials and details of NPs electrochemical synthesis were reported earlier [14]. The structural and morphological characterization of NPs–PAmHU systems was performed in solution, lyophilized powder and film.

The thin film samples were prepared by spin coating method, using a WS-400B-6NPP/LITE spin coater, deposited on microscope slide glass substrates with 25×25 mm^2 area.

Magnetic measurements of approximately 4 mg of lyophilised samples were carried out at room temperature (RT) by Vibrating Sample Magnetometer technique (VSM) with a MicroMag 2900/3900 Vibrating Sample; with the applied field between–10000 to +10000 Oe.

The AFM measurements were performed using a Solver Pro 7M instrument operated in tapping mode under ambient conditions. Standard silicone nitride tips (NSC21) with tip curvature radius of 10-20 nm were used.

The size distribution of PAmHU–NPs was determined using NIS Elements Basic Research imaging software. For each nanoparticle the average size is considered as the average of three measurements on three different directions.

The hydrodynamic diameter of PAmHU–NPs, was determined by using a Shimadzu - SALD-7001 Laser Diffraction Particle Size Analyser.

The FTIR spectra of NPs–PAmHU lyophilized powder were recorded in the range between 4000 and 400 cm^{-1} with a Tensor 10 Bruker spectrophotometer in order to confirm the magnetite atoms inter-bounds with PAmHU functional groups.

Thermogravimetric analysis (TGA) was performed on a Mettler Toledo model TGA/SDTA 851e analyzer. Approximately 3 mg of sample was accurately weighed into a 40-μL aluminum pan and sealed with a punched lid. An empty holed lid aluminium pan was used as a reference. The samples were heated from 25 to 900°C with 10°C/min heating rate under air atmosphere.

3. RESULTS AND DISCUSSIONS

Uniqueness of molecular arrangements at nanoscale level entail major changes in macroscopic magnetic properties, such as enhancements magnetocaloric effect, giant magnetoresistance, and quantum tunneling of magnetization [2]. This is due to interparticle interactions and finite size effects that are considered the most dominating factors on the magnetic behaviour of individual nanoparticles as their size decreases. The superparamagnetism (SPM) is a studied size effect because the particle anisotropy is generally proportional to its volume.

The magnetization, *M*, *versus* applied field, *H*, curves measured at RT for the lyophilized samples from bulk solutions of representative current densities galvanostatic regimes are presented in Figure 1. A tendency of *M* to decrease with the decrease of current density galvanostatic regime was observed. This effect may be a result of two factors; one is the decrease of the mass of magnetite electrosynthesized in the virtue of Faraday's first law of electrolysis. The other reason is the decrease of the size of magnetite crystallites in matrixes with the decrease of current density galvanostatic regime. The unsaturated magnetization profile curves also sustain these affirmations. We can conclude that the system exhibits a superparamagnetic to ferromagnetic behaviour (very low coercivity and remanence).

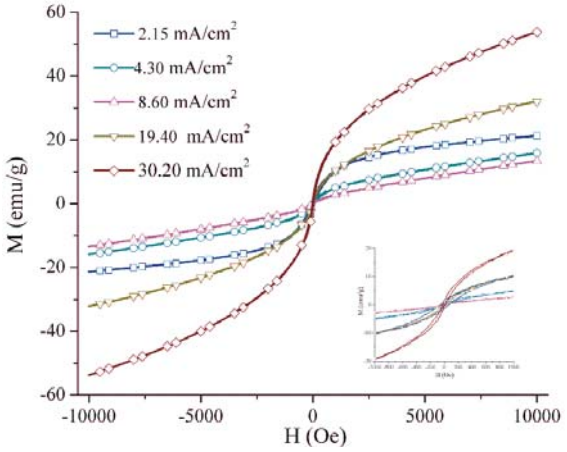

Fig. 1. The magnetization, *M*, *versus* applied field intensity, *H*, curves measured at RT of the magnetite – PAmHU lyophilized powders.

M versus H curves measured at RT of the magnetite–PAmHU lyophilized powders from bulk and cathode precipitate solutions of representative 30.20 mA/cm^2 current density are shown in Figure 2. The coercivity is present in the curve of precipitate. The saturation magnetization, M_s, of about 80 emg/g, is almost reached for this type of nanoparticles beyond 10 kOe. This phenomenon is explained by the fact that magnetic interactions between the crystallites exist because the crystallites are isolated in a matrix with a thin layer of polymer [16]. Contrarily, very low coercivity and remanence is present in the lyophilized powder from the bulk solution. These show that the PAmHU shell of the magnetic crystallite reduces the interaction by increasing the effective distance between magnetic grains and weakening or eliminating the exchange coupling between them. These conclusions are in accordance with obtained EPR results supposing that the phase is composed of clusters of crystallites that are covered, less or more, with a thick layer of PAmHU [14].

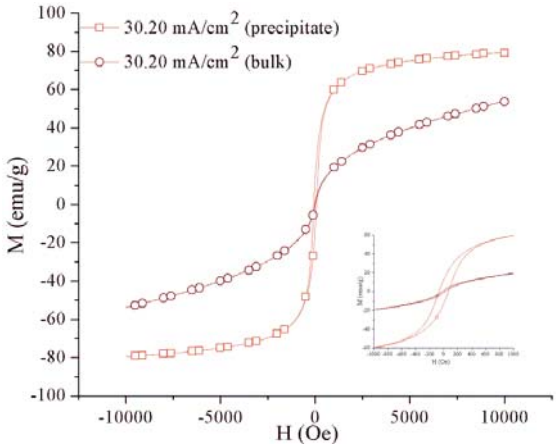

Fig. 2. The *M versus H* curves of the magnetite – PAmHU lyophilized powders from bulk solution and precipitate of electrosynthesis at 30.20 mA/cm^2 inset detail of hysteresis domain.

The 2D topography obtained by AFM film analysis, containing bulk phase suspension obtained at 30.20 mA/cm^2 is shown in Figure 3. Similarly, the AFM topography of the PAmHU was presented by Melnig *et al*. [13]. Comparing these results with those of the pure PAmHU it can be seen that the NPs are present in the form of clusters and are covered with polymer, which are in concordance with TEM results [14]. AFM analysis revealed a dimension distribution within 40 to 200 nm with a mean size of 119.89.

The diagrams of numerical size distribution of magnetite–PAmHU from bulk systems obtained by DLS are shown in Figure 4. In the case of PAmHU free synthesis the NPs diameter obtained by DLS was equal to 420 nm. These particles were not stable and in an interval of 2–3 hours were subjected to a conglomeration process.

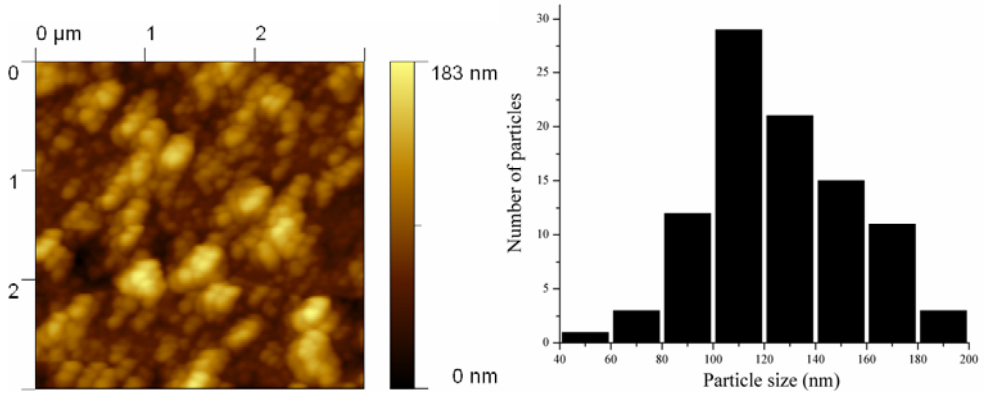

Fig. 3. The 2D topography (a), and dimensions bar chart distribution (b) of magnetite NPs obtained at 30.20 mA/cm^2.

For 8.60 and 19.40 mA/cm^2 current densities the distribution maximum was approximately at the same values, 87 nm respectively 96 nm. For 30.20 mA/cm^2 current density, the NPs dimensions of bulk suspension had a maximum at 25 nm, confirming the fact that NPs are seen as being out-flaking with a thin layer of polymer. This results are in agreement with magnetic measurements in case of magnetite–PAmHU lyophilized powders from bulk solutions (Fig. 1); the higher interaction from magnetite crystallites being observed in case of 30.20 mA/cm^2 current density because of thin layer of PAmHU. The flocculated magnetite that was straggled and suspended by sonication had the maximum of distribution at 96 nm. This shows that the resulted entities after sonication most probably form clusters of crystallites or, the crystallites are capped with a thick layer of polymer showing that the surface reactivity (affinity) of magnetite NPs is increased by the dispersion process. The first hypothesis is supported by magnetic measurements in case of magnetite–PAmHU lyophilized powders precipitated from cathode; the clusters consisting of crystallites that are isolated in the matrix with a thin layer of polymer showed ferromagnetic behaviour.

In order to confirm the bonding of PAmHU functional groups with magnetite atoms, the FTIR spectra of PAmHU, magnetite PAmHU free and PAmHU–magnetite NPs systems were investigated. Detailed IR analysis of PAmHU was presented by Melnig *et al*. [13].

The FTIR spectrum of magnetite PAmHU free has broad bands at 580 and 400 cm^{-1} corresponding to pure magnetite, which is in good agreement with Melnig and Ciobanu [12] and water absorption bands: 3600 – 2800 cm^{-1} and 1750 – 1300 cm^{-1} due to some hydrated quantity of water. The characteristic bands of PAmHU functional group region [4000 – 1700 cm^{-1}; figure 5(a)] and fingerprint region [1700 – 400 cm^{-1}; figure 5(b)], corroborated with correlation chart reveal that the regions of water absorption 3600 – 2800 cm^{-1} and 1800 – 1300 cm^{-1} are strongly affected by the presence of magnetite NPs.

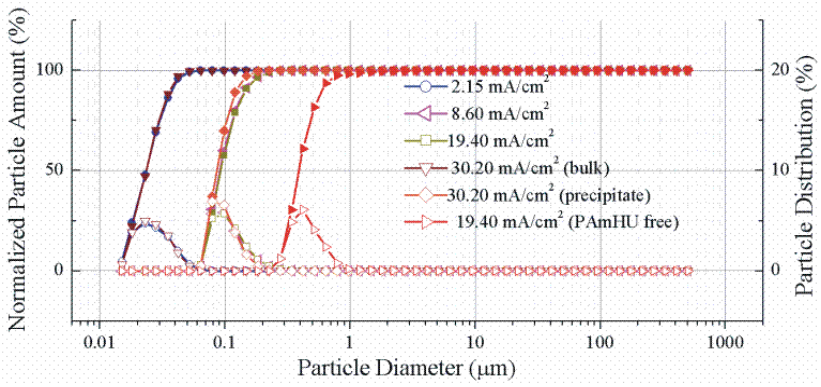

Fig. 4. Numerical size distribution of magnetite particles; particle distribution (%) (empty symbols), normalized particle amount (%) (filled symbols).

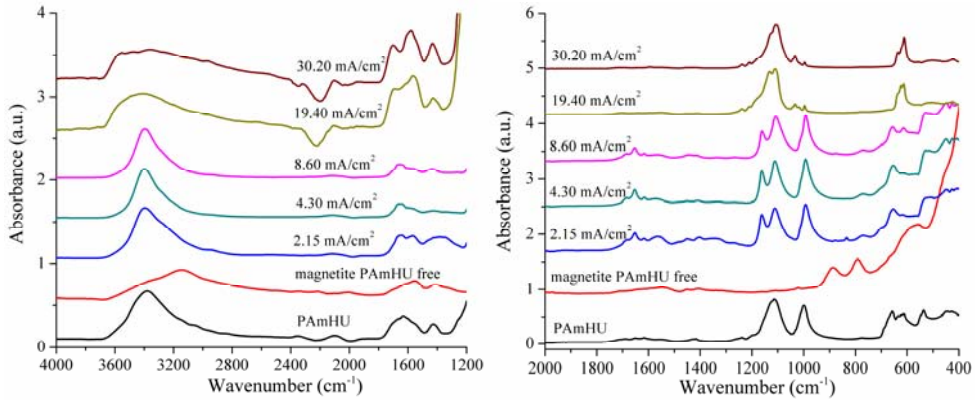

(a) (b)

Fig. 5. FTIR spectra of the PAmHU polymer and PAmHU-NPs; functional group (a) and fingerprint (b) extended domains.

These bands are given by the O–H fundamental stretching vibrations mode of water (with maximum at 3380 cm^{-1} for PAmHU, shifted backward to 3140 cm^{-1} for magnetite PAmHU free and forward to 3400 cm^{-1} for magnetite with PAmHU with flat peaks for 19.40 and 30.20 mA/cm^2) and O–H in plane bending mode (at around 1630 cm^{-1} for PAmHU).

These changes in bands could appear due to a small population of water bonded by hydrogen with PAmHU polymer, probably with the three possible proton acceptors groups: the ether oxygen, the urethane carbonyl oxygen and the acrylamide carbonyl oxygen.

As the result, amide peaks at 2350 and 2100 cm^{-1} changes their profile for 19.40 and 30.20 mA/cm^2. The peak at 1670 cm^{-1} appears due to vibrations of free C=O from urethane groups (hard segment), and the shoulder at 1628 cm^{-1} was

assigned to carbonyl groups involved in H bonding with the N–H groups of the urethane hard fragments which seems to be strongly affected for 19.40 and 30.20 mA/cm^2. At this specified current density it is also important to mention the peak at 1420 cm^{-1} corresponding to the wag mode of C–O–C and CH_2 bands from ether and ethyl respectively (soft segment) that changes their contribution due to the new folding possibility in the presence of the magnetite NPs.

The Fe–O bond stretching vibrations are noticeable at 520 cm^{-1}, apparently diminishing for 19.40 and 30.20 mA/cm^2 revealing the possibility of strongly interactions or changes in the crystal lattice of magnetite [9].

The representative TGA curves of PAmHU–magnetite NPs for 30.20 mA/cm^2 current density are presented in Figure 6. The TGA curves of pure PAmHU lyophilised powder from Figure 7 and magnetite thermal behaviour from literature can be regarded as references.

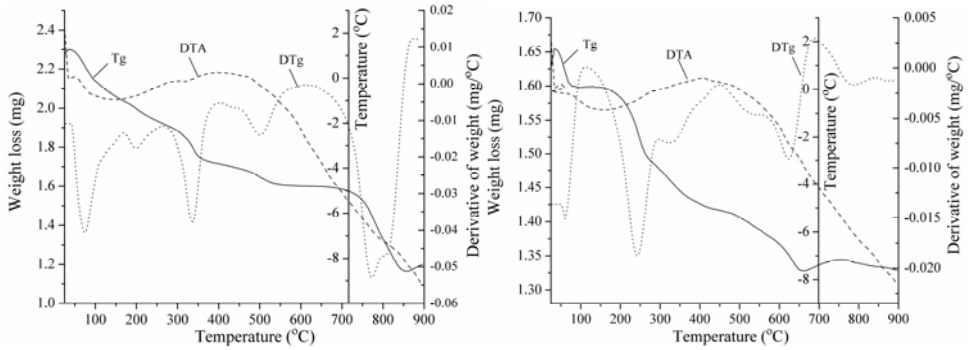

Fig. 6. TGA curves of PAmHU caped magnetite NPs for 30.20 mA/cm^2 current density galvanostatic regime synthesis: (a) lyophilised powder from bulk; (b) flocculated powder.

In Table 1 the characteristics of the thermal decomposition stages of analysed samples are summarized. In all three cases the weight loss within ambient to around RT < T < 100°C can be ascribed to water coordination desorption adsorbed by magnetite NPs or linked by PAmHU via hydrogen bonds. This hypothesis is also sustained by FTIR analysis.

Theoretically, between 100°C and 300°C the weight gain is ascribed to the oxidation of the magnetite to maghemite [5]. During the reaction the density of material falls and the weight increases because of oxygen uptake:

$$2Fe_3O_4 + 1/2\,O_2 \rightarrow 3\gamma - Fe_2O_3; \quad \Delta m_{theor} = 1.7\%.$$

This weight gain is observed in a restricted domain because of the release of strongly bound water and of the PAmHU degradation. If the endothermic stages around 100 to 200°C are attributed to the water release, then this process corresponds to the stages II of PAmHU and magnetite bulk sample, in the last case

the process being shifted to 233.51°C due to water release on magnetite and the stage III of random chain cleavage of PAmHU, as it can be seen from figure 6(a). In case of magnetite precipitate samples, these processes (of stage II) are not present separately, more possibly due the large magnetite content converted to maghemite, comparatively with the magnetite content from bulk, and of more complex water release and PAmHU chain cleavage processes, in the hypothesis of the magnetite crystallites aggregates.

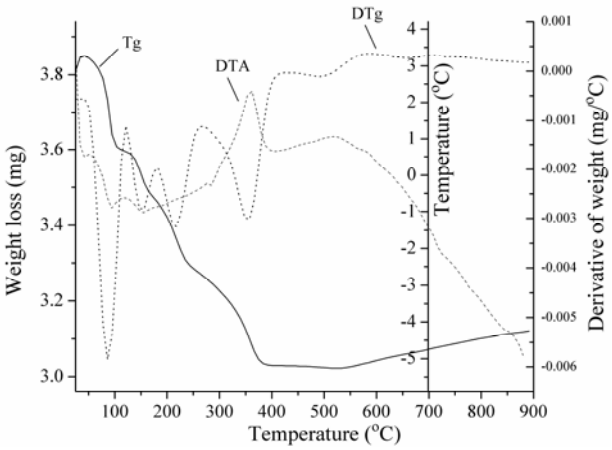

Fig. 7. Thermal behaviour of the PAmHU powder.

Table 1
Thermal decomposition stages characteristics of magnetite lyophilised powder from bulk and flocculated, and PAmHU lyophilised powder

Sample	Stage	T_{onset}	T_{peak}	T_{endset}	W(%)	Residue(%)
Magnetite (precipitate) (30.20 mA/cm^2)	I	48.44	60.87	73,28	3.45	79.84
	II	191.78	242.9	261,22	7.31	
	III	318.78	328.41	391,09	3.96	
	IV	498.06	622.41	730.59	5.46	
Magnetite (bulk) (30.20 mA/cm^2)	I	49.41	66.65	107.55	11.71	49.95
	II	183.78	197.78	233.51	5.35	
	III	303.91	338.60	351.11	8.83	
	IV	435.55	501.58	534.38	4.94	
	V	732.72	769.53	850.5	19.22	
PAmHU	I	61.01	85.92	96.51	6.66	78.3
	II	138.14	148.58	158.63	3.80	
	III	198.04	217.29	234.39	4.86	
	IV	327.30	361.90	380.62	6.38	

The oxidation of magnetite to maghemite involves the reduction of Fe atoms per unit cell from 24 in magnetite to 21⅓ in maghemite. The reaction proceeds by migration of the cations towards the surface of the crystal together with the creation

of cation vacancies [15] at the surface, the cations are oxidized and interact with adsorbed oxygen to form rim of maghemite. The diffusion coefficient for cation migration is ~$2 \cdot 10^{-15}$ cm^2/s. In small crystals, the diffusion pathways are short and reaction rates fast conducting rapidly to complete oxidation. In contrast in larger crystals diffusion pathways are so long that the temperature must be raised above 500°C.

At ~220°C the outer layer of maghemite blocks any further conversion at this temperature. Beyond $T > 300$°C, the structural strain arising as a results of the oxidation process caused by the spontaneous nucleation of hematite (α-Fe_2O_3) in the maghemite (γ-Fe_2O_3) layer [6]. At temperatures higher than 400°C, the remaining magnetite is transformed directly into hematite.

The magnetite bulk powder (Figure 6a) has a larger weight loss (there is a similar case reported by Purushotham *et al*. [17]) confirming the intimated processes conversion per each small particle. In case of magnetite precipitate powder (Figure 6b) the presumption of aggregation in clusters of crystallites leads to the idea that the thermal disaggregation of clusters conduct to PAmHU shielded nanoclusters and the oxidation of magnetite is closer to that of pristine magnetite. This hypothesis is confirmed also by the residue, which is smaller in magnetite bulk samples while in the magnetite precipitate samples it is higher than in the PAmHU powder.

4. CONCLUSIONS

Magnetite NPs surface-functionalized with PAmHU, obtained by one step electrochemical synthesis route [14], show the following features.

The core magnetic properties have superparamagnetic to ferromagnetic behaviour (very low coercivity and remanence) depending on the provenance of clustering NPs: from bulk solution or cathode precipitate product.

The morphology and structural analysis of the magnetite–PAmHU functionalised NPs confirm the covered of magnetic-cores with polymer.

According to these studies the synthesised NPs seem to form a PAmHU–clustering system, with an inner-core consisting of magnetite unit entities (crystallites).

These NPs are water soluble, stable and biocompatible due to the PAmHU polymer that out-flaking them, being suitable for many applications.

Acknowledgments. This work was supported by European Social Fund – „Cristofor I. Simionescu" Postdoctoral Fellowship Programme (ID POSDRU/89/ 1.5/S/55216), Sectoral Operational Programme Human Resources Development 2007 – 2013.

REFERENCES

1. ASTALAN A.P., AHRENTORP F., JOHANSSON C., LARSSON K., KROZER A., *Biomolecular reactions studied using changes in Brownian rotation dynamics of magnetic particles*, Biosens. Bioelectron., 2004, **19**, 945–951.

2. BATLLE X., LABARTA A., *Finite-size effects in fine particles: magnetic and transport properties*, J. Phys. D: Appl. Phys., 2002, **35**, R15–R42.
3. BERRY C.C., *Possible exploitation of magnetic nanoparticle-cell interaction for biomedical applications*, J. Mater. Chem., 2005, **15**, 543–547.
4. DOBSON J., *Magnetic nanoparticles for drug delivery*, Drug. Develop. Res., 2006, **67**, 55–60.
5. FRANGER S., BERTHET P., DRAGOS O., *Large influence of the synthesis conditions on the physico-chemical properties of nanostructured Fe_3O_4*, J. Nanopart. Res., 2007, **9**, 389–402.
6. GALLAGHER K.J., FEITKNECHT W., MANNWEILER U., *Mechanism of oxidation of magnetite to γ-Fe_20_3*, Nature, 1968, **217**, 1118–1121.
7. GASS J., PODDAR P., ALMAND J., SRINATH S., SRIKANTH H., *Superparamagnetic polymer nanocomposites with uniform Fe_3O_4 nanoparticle dispersions*, Adv. Funct. Mater., 2006, **16**, 71–75.
8. JIN H., HONG B., KAKAR S.S., KANG K.A., *Tumor-specific nano-entities for optical detection and hyperthermic treatment of breast cancer*, Adv. Exp. Med. Biol., 2008, **614**, 275–284.
9. KEISER J.T., BROWN C.W., HEIDERSBACH R.H.J., *The electrochemical reduction of rust films on weathering steel surfaces*, Electrochem. Soc., 1982, **129**, 2686–2689.
10. LANDFESTER K., RAMIREZ L.P., *Encapsulated magnetite particles for biomedical application*, J. Phys. Condens. Mat., 2003, **15**, S1345–S1361.
11. LEE J., ISOBE T., LENNA M., *Magnetic properties of ultrafine magnetite particles and their slurries prepared via in-situ precipitation*, Colloids Surf. A, 1996, **109**, 121–127.
12. MELNIG V., CIOBANU C., *Characterization of water-soluble polyamidhydroxyurethane for biological applications*, J. Optoelectron. Adv. Mater., 2005, **7**, 2809–2815.
13. MELNIG V., APOSTU M.O., FOCA N., *Polymer assisted synthesis of water soluble PbSe Quantum Dots*, J. Nanopart. Res., 2008, **10**, 171–177.
14. MELNIG V., URSU L., *Poly(amidehydroxyurethane) template magnetite NPs electrosynthesis: I. Electrochemical aspects and identification*, J. Nanopart. Res. 2010, **13**, 2509–2523.
15. MICHEL A., BÉNARD J., *Chimie minérale*, Masson, Paris, 1964.
16. MORALES M.P., VEINTEMILLAS-VERDAGUER S., MONTERO M.I., SERNA C.J., ROIG A., CASAS L., MARTINEZ B., SANDIUMENGE F., *Surface and internal spin canting in γ-Fe2O3 NPs*, Chem. Mater., 1999, **11**, 3058–3064.
17. PURUSHOTHAM S., CHANG P.E.J., RUMPEL H., KEE I.H.C., NG R.T.H., CHOW P.K.H., TAN C.K., RAMANUJAN R.V., *Thermoresponsive core–shell magnetic NPs for combined modalities of cancer therapy*, Nanotechnology, 2009, **20**, 305101–305112.
18. SUN C., VEISEH O., GUNN J., FANG C., HANSEN S., LEE D., SZE R., ELLENBOGEN R.G., OLSON J., ZHANG M., *In vivo MRI detection of gliomas by chlorotoxin-conjugated superparamagnetic nanoprobes*, Small., 2008, **4**, 372–379.
19. YANG P.F., LEE C.K., *Hyaluronic acid interaction with chitosan-conjugated magnetite particles and its purification*, Biochem. Eng. J., 2007, **33**, 284–289.

Received May 7, 2013